Noncoherent Detection for an EM-Lens-Enabled Massive MIMO System

George Yammine[1], Stephan Bucher[2], Robert F.H. Fischer[1]
[1]Institut für Nachrichtentechnik, [2]Institut für Mikrowellentechnik, Universität Ulm, Ulm, Germany
Email: {george.yammine, stephan.bucher, robert.fischer}@uni-ulm.de

***Abstract*—In multi-user massive MIMO uplink scenarios, noncoherent detection schemes are an attractive low-complexity alternative to channel-estimation-based equalization. Since phase information is not available at the receiver, the spatial separation of the induced power is used to resolve the different users. In case of no spatial separation, noncoherent detection is not possible. In this paper, we employ antenna arrays where an electromagnetic lens is placed in front of the antenna elements to focus the induced power to a smaller footprint. This results in a spatial separation required for noncoherent detection. The performance of the EM-lens-enabled system is assessed by means of numerical simulations.**

I. Introduction

As the demand for spectral and power efficiency increases, *massive MIMO* systems equipped with a very large number of antennas have attracted growing attention [6], [8]. In the uplink, a small number of users communicate with a central base station. In order to exploit the benefits of such systems, accurate estimation of the channel coefficients (by means of training sequences/pilot symbols) is required. However, when learning the channel, there may be interference from other users due to pilot contamination arising from the reuse of the training sequences [4]. In order to avoid channel estimation, noncoherent approaches can be applied [10], which include noncoherent detection of the users (by means of decision-feedback differential detection) and multi-user interference mitigation [5] (using noncoherent decision-feedback equalization). However, these techniques rely on the separability of the users based on the per-user received power induced on the antenna array. In case spatial separation is not feasible, then noncoherent detection fails.

In this paper, we employ an *electromagnetic lens* at the receiver array, as proposed in [13]. The lens focuses the received power induced by each transmitter onto a small subset of antennas at the base station. The usage of the lens provides the spatial separation required for noncoherent detection. We compare the performance of noncoherent detection with that of coherent by means of numerical simulations in various settings and analyze different operation scenarios. We show that for suited system design the performance of noncoherent detection is similar to that of coherent detection with perfect channel knowledge.

The paper is organized as follows. In Section II, we define the scenario and present the channel model. We briefly recapitulate the employed noncoherent detection algorithm in Section III. In Section IV, numerical simulation results are presented. Finally, conclusions are drawn in Section V.

This work was funded by the Deutsche Forschungsgemeinschaft (DFG, German Research Foundation) — FI 982/12-1 and WA 3506/5-1.

II. System Model

We consider a multi-user uplink system where N_{u} single-antenna users transmit to a central base station equipped with $N_{\mathsf{rx}} \gg N_{\mathsf{u}}$ antennas, a so-called massive MIMO system [6].

In each time step k, each user u transmits a differentially encoded unit-magnitude phase-shift keying (DPSK) symbol $b_{k,u}$. The transmit symbols are generated from the quaternary PSK data symbols $a_{k,u}$ (the symbols $a_{k,u}$ and $b_{k,u}$ are drawn from the set $\mathcal{M} \stackrel{\text{def}}{=} \{1, \mathrm{j}, -1, -\mathrm{j}\}$) as [10]

$$b_{k,u} = a_{k,u} b_{k-1,u} \ , \quad b_{0,u} = 1 \ . \tag{1}$$

At the receiver, noncoherent detection is applied (cf. Sec. III).

A. Far-Field Model

In previous work, we employed a geometrical channel model based on the assumption that the users are placed at a relatively close distance d_{u} (in relation to the aperture of the array) to the linear antenna array at the receiver. This results in the received power of the individual users induced on the antenna array that are well approximated as a Gaussian bell shape [10], [12]. We denote the power distribution as the user-specific *power-space profile (PSP)* $P_{m,u} \stackrel{\text{def}}{=} \mathrm{E}\{|h_{m,u}|^2\}$. For noncoherent detection, the different users are detected based on the spatial separation characterized by the PSPs.

As d_{u} increases, the ability to separate the users is lost since the PSPs of all the users become similar (flatten out into a uniform profile) and cover all the antennas at the receiver.

To model the new channel scenario, the following is assumed. The uniform antenna array is deployed along the y-axis, centered at $y = 0$ and the antennas are numbered as $m = 1, \ldots, N_{\mathsf{rx}}$ with antenna spacing of d_{a}. On the y-axis, each antenna is positioned at

$$y_m \stackrel{\text{def}}{=} -\frac{N_{\mathsf{rx}} - 1}{2} d_{\mathsf{a}} + (m-1) d_{\mathsf{a}} \ . \tag{2}$$

For even N_{rx}, the array spans a length $2D_{\mathsf{a}}$ ($-D_{\mathsf{a}}$ to D_{a}, cf. Fig. 1) with

$$D_{\mathsf{a}} \stackrel{\text{def}}{=} \frac{N_{\mathsf{rx}}}{2} d_{\mathsf{a}} \ . \tag{3}$$

We also assume that the users are located far enough from the receiver such that the *far-field* assumption holds. In this

DOI: 10.30420/454862030

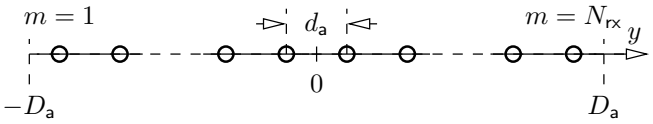

Figure 1. Uniform linear array (ULA) with N_rx antennas (even). The array is centered at $y = 0$ and spans a length of $2D_\mathsf{a}$.

case, planar waves with angle of arrival θ_u impinge on the antenna array. If only a single path from each user to the array is present, the channel coefficient (in complex baseband notation) between user u and antenna m is given by

$$h_{m,u} \overset{\text{def}}{=} h_{u,\theta_u} \, \mathrm{e}^{-\mathrm{j}\frac{2\pi}{\lambda}(m-1)d_\mathsf{a}\sin(\theta_u)} \, , \tag{4}$$

where $h_{u,\theta_u} \overset{\text{def}}{=} h_u \cos(\theta_u)$ is the channel gain including the aperture loss effect of the antenna, and λ is the free-space wavelength of the signal. Power control is applied at each transmitter, such that the total receive power per user is $P_\mathsf{rx} \overset{!}{=} 1$. We also assume that the user u has (infinitely many) local scatterers. Therefore, h_u is a zero-mean complex Gaussian random variable with variance $1/N_\mathsf{rx}$.

For a given angle of arrival θ_u, only part of the planar wave (power flux density) is captured by the antenna array (cf. Fig. 2). Integrating the power flux density over the array, we see that the antenna aperture scales with $\cos(\theta_u)$.

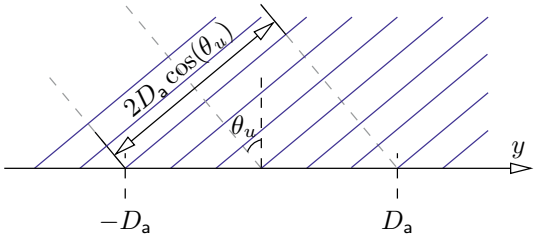

Figure 2. Depiction of the captured power coming from a planar wave (blue) having an angle of arrival θ_u.

The function

$$\alpha_m(\theta_u) \overset{\text{def}}{=} \mathrm{e}^{-\mathrm{j}\frac{2\pi}{\lambda}(m-1)d_\mathsf{a}\sin(\theta_u)} \tag{5}$$

represents the phase of the arriving signal at each antenna m (using antenna $m = 1$ as reference). This is a direct consequence of the distance the signal travels until its wavefront reaches each antenna (cf. Fig. 3). The function $\alpha_m(\theta_u)$ is commonly known as the *array response*.

Due to planar waves (uniform power-space profile) arriving at the array, noncoherent multi-user detection is not possible. In order to counteract this effect, a new approach is required.

In the literature, an *electromagnetic (EM) lens* at the base station has been proposed [13], which is placed in front of the antennas, cf. Fig. 4.

The EM lens can be implemented as a dielectric lens with specially designed surface curvatures [3], [9], or a planar lens consisting of multiple phase shifters [2]. This concept is not only theoretical, but also practically implementable, especially

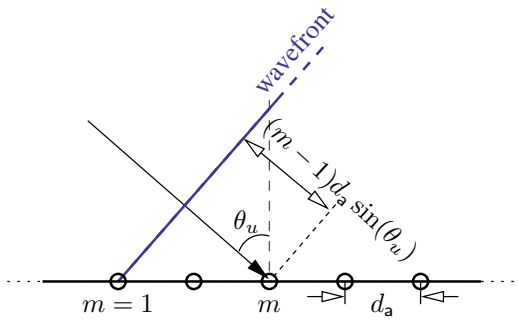

Figure 3. Array response for a uniform linear antenna configuration. The wavefront of the signal is depicted in blue.

at higher carrier frequencies. One such EM-lens system has been already realized, cf. [14].

The EM lens focuses the received power induced by each user onto a smaller set of antenna elements (footprint) at the receiver. When the users are sufficiently spaced, their specific footprints do not overlap, thus creating interference free channels (i.e., perfect user separation).

B. EM-Lens-Enabled Massive MIMO Channel

To include the effects of the EM lens [3], [9], the construction in [13] is employed to calculate the power-space profile vector $\boldsymbol{p}_u$. First, the spatial position $\bar{y}_{\theta_u}$ of the maximum power induced by the user u for a given angle of arrival θ_u is calculated according to

$$\bar{y}_{\theta_u} = \frac{\theta_u}{\Theta} \, , \tag{6}$$

where Θ is the *coverage angle* of the array,[1] i.e., $\theta_u \in \left[-\frac{\Theta}{2}, \frac{\Theta}{2}\right]$. The fraction of the power collected by antenna m is approximated by

$$p_m^{(\theta_u)} \overset{\text{def}}{=} \int_{y_m - d_\mathsf{a}/2}^{y_m + d_\mathsf{a}/2} \mathsf{f}_Y^{(\theta_u)}(y) \, \mathrm{d}y \, , \tag{7}$$

where $\mathsf{f}_Y^{(\theta_u)}(y)$ is the *normalized power density function*, with $\int_{-D_\mathsf{a}}^{D_\mathsf{a}} \mathsf{f}_Y^{(\theta)}(y) \, \mathrm{d}y = 1$.

This means that the EM lens changes only the induced signal power distribution. The sum power collected by the array with and without the EM lens remains the same. Eq. (7) together with the normalization lead to

$$\sum_{m=1}^{N_\mathsf{rx}} p_m^{(\theta_u)} \overset{!}{=} 1 \tag{8}$$

for any power-space profile vector $\boldsymbol{p}_u$.

Using the lens design from [13], the normalized power density function is approximated by

$$\mathsf{f}_Y^{(\theta_u)}(y) = \frac{1}{\sqrt{2\pi V}} \, \mathrm{e}^{-\frac{(y-\bar{y}_{\theta_u})^2}{2V}} \, , \tag{9}$$

[1]The lens is designed such that as long as the user is within the base station coverage angle, the induced power is focused on the array elements, i.e., no receive power is lost.

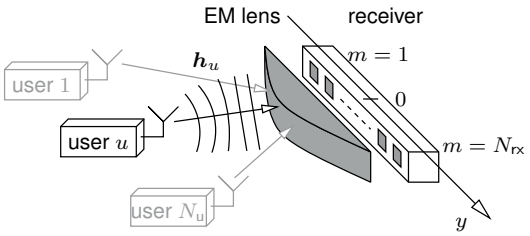

Figure 4. Multi-user massive MIMO uplink system with EM-lens-enabled antenna array. N_{u} users transmit to a central base station with $N_{\mathsf{rx}} \gg N_{\mathsf{u}}$ antennas. The users are located far enough such that the far-field assumption holds and plane waves impinge on the array. The array is centered at $y = 0$.

i.e., the power focused on the array follows a Gaussian bell shape, where $\bar{y}_{\theta_u}$ is the position of the maximum of the power density and V is the variance. In essence, the variance denotes the width of the beam that is focused on the array. Instead of specifying V, a 90% *power beamwidth*[2] Δ, which characterizes the focusing parameter of the lens can be defined. Due to the Gaussian assumption $\Delta^2 = 18.42V$ holds. Replacing (9) in (7), we can derive a closed-form formula for the fraction of the power collected by antenna m as

$$\begin{aligned} p_m^{(\theta_u)} &= \int_{y_m - d_{\mathsf{a}}/2}^{y_m + d_{\mathsf{a}}/2} \frac{1}{\sqrt{2\pi V}} \, \mathrm{e}^{-\frac{(y-\bar{y}_{\theta_u})^2}{2V}} \, \mathrm{d}y \\ &= \mathrm{Q}\left(\frac{y_m - d_{\mathsf{a}}/2 - \bar{y}_{\theta_u}}{\sqrt{V}} \right) \\ &\quad - \mathrm{Q}\left(\frac{y_m + d_{\mathsf{a}}/2 - \bar{y}_{\theta_u}}{\sqrt{V}} \right) , \end{aligned} \tag{10}$$

where $\mathrm{Q}(\cdot)$ is the complementary Gaussian integral function. When no lens is present, the power collected by the array is uniformly distributed over all antennas, i.e., $p_m = 1/N_{\mathsf{rx}},\ m = 1, \ldots, N_{\mathsf{rx}},\ \forall \theta_u$.

Given the power redistribution function, the channel coefficients between user u and antenna m for the array using the lens are then given as

$$\begin{aligned} h_{m,u,\mathsf{lens}} &\overset{\text{def}}{=} h_{m,u} \sqrt{N_{\mathsf{rx}} p_m^{(\theta_u)}} \qquad (11) \\ &= h_{u,\theta_u} \sqrt{N_{\mathsf{rx}} p_m^{(\theta_u)}} \, \mathrm{e}^{-\mathrm{j}\frac{2\pi}{\lambda}(m-1)d_{\mathsf{a}} \sin(\theta_u)} \\ &= h_u \cos(\theta_u) \sqrt{N_{\mathsf{rx}} p_m^{(\theta_u)}} \, \alpha_m(\theta_u) \, . \qquad (12) \end{aligned}$$

In view of block processing, we define the (column) channel coefficients vector of user u to the antenna array without the lens as

$$\boldsymbol{h}_u \overset{\text{def}}{=} [h_{1,u}, \, h_{2,u}, \, \ldots, \, h_{N_{\mathsf{rx}},u}]^{\mathsf{T}} \, , \tag{13}$$

and

$$\boldsymbol{g}_u \overset{\text{def}}{=} \left[\sqrt{N_{\mathsf{rx}} p_1^{(\theta_u)}}, \, \sqrt{N_{\mathsf{rx}} p_2^{(\theta_u)}}, \, \ldots, \, \sqrt{N_{\mathsf{rx}} p_{N_{\mathsf{rx}}}^{(\theta_u)}} \right]^{\mathsf{T}} \, , \tag{14}$$

[2]We define the 90% beamwidth such that at the positions $\bar{y}_{\theta_u} \pm \Delta$, the power drops to 0.1 times the power at $\bar{y}_{\theta_u}$.

as the vector of the square roots of the normalized power fractions (i.e., the lens power-distribution vector or gain vector). To include the effects of the EM lens on the channel vector, we have (cf. (11))

$$\boldsymbol{h}_{u,\mathsf{lens}} \overset{\text{def}}{=} \boldsymbol{G} \boldsymbol{h}_u \, , \tag{15}$$

where $\boldsymbol{G} = \mathbf{diag}(\boldsymbol{g})$ is the diagonal gain matrix. We denote this channel model as the single-path EM-lens-enabled channel model.

When choosing $\boldsymbol{G} = \boldsymbol{I}$, the channel model when no lens is present ($p_m = 1/N_{\mathsf{rx}},\ m = 1, \ldots, N_{\mathsf{rx}},\ \forall \theta_u$) is obtained.

C. L-Path Model

The L-path EM-lens-enabled channel model is an extension of the single-path model with L paths per user each having a random deviation $\varphi_{u,\ell},\ \ell = 1, \ldots, L$, from the nominal (main) angle of arrival θ_u, i.e., $\theta_{u,\ell} = \theta_u + \varphi_{u,\ell}$. This deviation is random, and it is well approximated by a zero-mean Gaussian random variable with variance σ_Φ^2, which denotes the angular spreading factor of the signal [15].

For each path ℓ between user u and antenna m, the channel coefficients are given by

$$\begin{aligned} h_{m,u,\ell} \overset{\text{def}}{=} h_{u,\ell} \cos(\theta_u + \varphi_{u,\ell}) \sqrt{N_{\mathsf{rx}} p_m^{(\theta_u + \varphi_{u,\ell})}} \\ \mathrm{e}^{-\mathrm{j}\frac{2\pi}{\lambda}(m-1)d_{\mathsf{a}} \sin(\theta_u + \varphi_{u,\ell})} \, . \end{aligned} \tag{16}$$

We assume that the channel coefficients from each path are independent of each other. Keeping the receive power induced on the array the same as in the single-path case, the total channel coefficient for antenna m reads

$$h_{m,u} = \frac{1}{\sqrt{L}} \sum_{\ell=1}^{L} h_{m,u,\ell} \, . \tag{17}$$

The power collected by each antenna m is calculated for each path via (6) and (10), where θ_u is replaced by $\theta_u + \varphi_{u,\ell}$; the overall collected power, i.e., the power-space profile vector $\boldsymbol{p}_u$, is then the average of all

$$p_m^{(\theta_u)} \overset{\text{def}}{=} \frac{1}{L} \sum_{\ell=1}^{L} p_m^{(\theta_u + \varphi_{u,\ell})} \, . \tag{18}$$

When the deviation angle $\varphi_{u,\ell}$ for each path is small, the resulting profile remains similar to the single-path model one, but is slightly broadened.

III. Noncoherent Detection

At the receiver, block processing is performed. We assume that the channel coefficients are randomly chosen according to (12) or (17) and remain constant over each transmission burst of N_{bl} symbols.

We form the receive block $\boldsymbol{R}$ by collecting N_{bl} time steps over N_{rx} antennas. This matrix can be written as

$$\boldsymbol{R} = \sum_{u=1}^{N_{\mathsf{u}}} \boldsymbol{h}_u \boldsymbol{b}_u^{\mathsf{T}} + \boldsymbol{N} \, , \tag{19}$$

ISBN 978-3-8007-4862-4

where $\boldsymbol{h}_u$ (or $\boldsymbol{h}_{u,\mathsf{lens}}$ when the EM lens is present) is the channel coefficients vector, $\boldsymbol{b}_u^{\mathsf{T}} \stackrel{\text{def}}{=} [b_{0,u}, \ldots, b_{N_{\mathsf{bl}}-1,u}]$ contains the transmit symbols of user u, and the matrix $\boldsymbol{N}$ collects the zero-mean circular-symmetric complex Gaussian noise samples $n_{m,k}$ with variance σ_{n}^2.

Decision-Feedback Differential Detection (DFDD) [1] of user u is then based on the $N_{\mathsf{bl}} \times N_{\mathsf{bl}}$ *correlation matrix* of the symbols (details about the algorithm can be found in [10])

$$\boldsymbol{Z}_u \stackrel{\text{def}}{=} \boldsymbol{R}^{\mathsf{H}} \boldsymbol{W}_u \boldsymbol{R} \,, \tag{20}$$

where $\boldsymbol{W}_u$ is the user-specific diagonal weighting matrix

$$\boldsymbol{W}_u \stackrel{\text{def}}{=} \mathbf{diag}(w_{1,u}, \ldots, w_{N_{\mathsf{rx}},u}) \,, \quad w_{m,u} \in [0,1] \,. \tag{21}$$

The matrix $\boldsymbol{W}_u$ is effectively a spatial-domain filter. There are several approaches for choosing the weighting coefficients, such as matched weighting and antenna windowing [10]. Another approach is to numerically optimize the weights using the inverse of the *signal-to-noise-plus-interference ratio* [5] as the cost function of the minimization problem (further information can be found in [12]). Under the assumption that the EM lens provides perfect user separation (i.e., the users are still sufficiently spaced that their PSPs do not overlap), this problem can be simplified to the minimization problem of the inverse signal-to-noise ratio of each individual user.

In case of the L-path model scenario, when the spreading factor σ_Φ^2 is small (it was shown in [7] that for an uplink scenario, the angle of arrival of the signal has an angular spread in the 2° to 5° range), we numerically optimize $\boldsymbol{W}_u$ for the nominal direction θ_u.

IV. Simulation Results

Numerical simulations were conducted for an $N_{\mathsf{u}} = 3$ multi-user scenario, with an $N_{\mathsf{rx}} = 100$ uniform linear antenna array. We set the inter-antenna spacing to $d_{\mathsf{a}} = \lambda/2$. The users and the base station employ omni-directional antennas, and transmit a block length of $N_{\mathsf{bl}} = 201$ using quaternary DPSK. The base station has a coverage angle of $\Theta = \frac{2}{3}\pi$, i.e., the array can see users having an angle of arrival $\theta_k \in [-\frac{\pi}{3}, \frac{\pi}{3}]$.

Each user was placed such that for $\Delta = 3\lambda$ (the value is given in [13]; for an antenna spacing of $\lambda/2$, 5 to 7 antennas are spotlighted) user 1 (■) would have been located in front of antenna $m_1 = 20$ ($\theta_1 = -0.34\Theta$), user 2 (■) in front of antenna $m_2 = 50$ ($\theta_2 = 0$), and user 3 (■) in front of antenna $m_3 = 85$ ($\theta_3 = 0.39\Theta$), if no lens were present (the user positions were kept comparable to the previous work, e.g., [12]).

The *signal-to-noise ratio (SNR)* is defined as E_{s}/N_0 ($N_0/2$ is the two-sided noise power spectral density). Due to PSK signaling, the SNR reads $E_{\mathsf{s}}/N_0 = 1/\sigma_{\mathsf{n}}^2$.

A. Single-Path Channel

First we compare the simulation results of the symbol error rate (SER) vs. the SNR of the single-path model, cf. Fig. 5. In case of coherent detection, perfect channel knowledge is assumed at the receiver. Detection is performed via maximum-ratio combining (MRC). The plots for the systems with and without the EM lens overlap exactly.

In case of noncoherent detection, the required coefficients of the per-user weighting matrix $\boldsymbol{W}_u$ were obtained for maximum SINR, followed by DFDD operating on the correlation matrix. When no lens is present (gray; solid), noncoherent detection is not possible. This is due to the uniform power profile seen at the receiver and user separation is not possible.

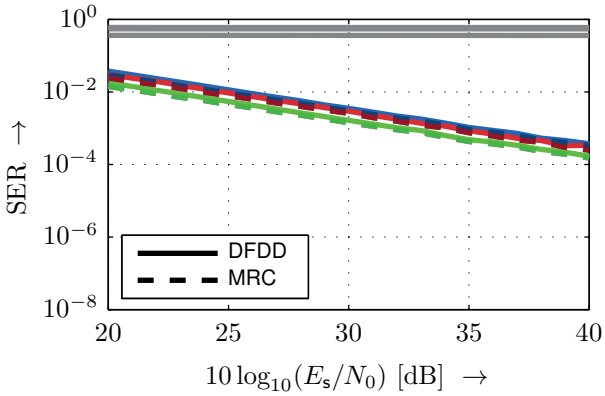

Figure 5. Symbol error rate vs. SNR for the multi-user scenario. $N_{\mathsf{u}} = 3$. Single-path model. Inter-antenna spacing $d_{\mathsf{a}} = \lambda/2$. $\Delta = 3\lambda$. user 1 (■): $m_1 = 20$ ($\theta_1 = -0.34\Theta$), user 2 (■): $m_2 = 50$ ($\theta_2 = 0$), user 3 (■): $m_3 = 85$ ($\theta_3 = 0.39\Theta$). Solid: DFDD (noncoherent); dashed: MRC (coherent). Gray plots are for the system without the EM lens.

In case of the system with the EM lens, we see that both noncoherent and coherent detection perform similarly. Noteworthy, since this is a single-path system model, we observe a diversity order of one. Here, the only source of randomness is the channel coefficient h_u, i.e., we have only one degree of freedom. Essentially, we see a SISO fading channel. The difference in performance between the users comes from the array aperture, i.e., the loss is proportional to the angle of arrival θ_u.

Next, we assess the performance (at $E_{\mathsf{s}}/N_0 \mathrel{\widehat{=}} 34$ dB) when the position of user 2 is varied along the array (by changing the angle of arrival θ_2). The results can be seen in Fig. 6. As expected, the farther the user is placed away from boresight ($\theta_u = 0$), the worse the performance. This is due to the aperture loss of the antenna array. In case of noncoherent detection, as user 2 (■) approaches the other users, we see a degradation in performance. This is a direct result of the user-specific footprints starting to overlap, and user separation starts to fail. In case of MRC, detection fails only when the user positions are exactly the same. In all other cases, it is impossible to separate the users based on phase information.

B. Two-Path Channel

Next, we conduct the same simulations as above, this time for the two-path model, with a spreading factor of $\sigma_\Phi^2 = 5°$; the remaining parameters are unchanged.

The SER vs. the SNR is plotted in Fig. 7. As expected, noncoherent detection without the EM lens (gray; solid)

ISBN 978-3-8007-4862-4

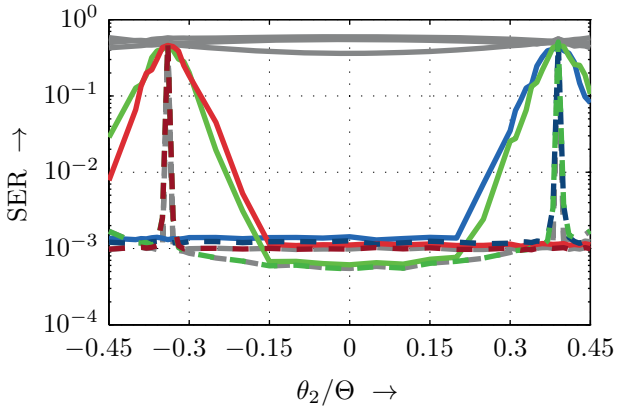

Figure 6. Symbol error rate vs. θ_2/Θ for the multi-user scenario. $N_\mathrm{u} = 3$. Single-path model. Inter-antenna spacing $d_\mathrm{a} = \lambda/2$. $\Delta = 3\lambda$. $E_\mathrm{s}/N_0 \mathrel{\widehat{=}} 34$ dB. user 1 (■): $m_1 = 20$ ($\theta_1 = -0.34\Theta$), user 3 (■): $m_3 = 85$ ($\theta_3 = 0.39\Theta$). The position of user 2 (■) is varied between -0.45Θ to 0.45Θ. Solid: DFDD (noncoherent); dashed: MRC (coherent). Gray plots are for the system without the EM lens.

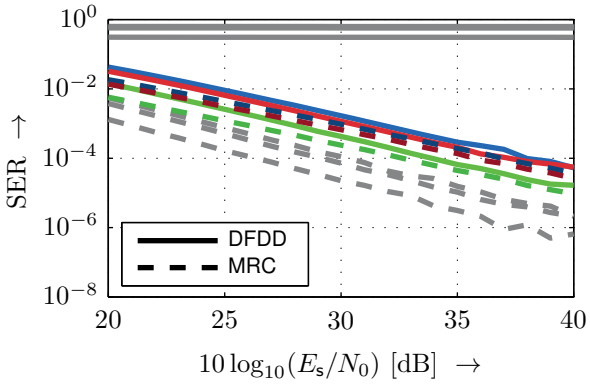

Figure 7. Symbol error rate vs. SNR for the multi-user scenario. $N_\mathrm{u} = 3$. Two-path model. Inter-antenna spacing $d_\mathrm{a} = \lambda/2$. $\Delta = 3\lambda$. user 1 (■): $m_1 = 20$ ($\theta_1 = -0.34\Theta$), user 2 (■): $m_2 = 50$ ($\theta_2 = 0$), user 3 (■): $m_3 = 85$ ($\theta_3 = 0.39\Theta$). Solid: DFDD (noncoherent); dashed: MRC (coherent). Gray plots are for the system without the EM lens.

again fails, and the performance of noncoherent detection and coherent using MRC perform is very similar. Compared to the results of Fig. 5, a higher diversity order is visible. Noteworthy, the diversity order is smaller than two even though two independent paths are active. This can be explained as follows: The channel coefficients of neighboring antennas are highly correlated, while the coefficients of antennas that are far apart are uncorrelated. Thus we do not have fully independent observations to fully exploit the diversity of the channel.

In each case, the performance is limited by the diversity order of the channel and not by the receive array. Coherent detection without the EM lens (gray; dashed), performs better than with the lens. Hence, coherent and noncoherent reception exhibit contrary behavior w.r.t. the application of the lens. For the noncoherent setting, the lens is the enabler, for the coherent case, it slightly degrades the performance.

Finally, the SER performance vs. the position of the middle user is plotted for the two-path channel model in Fig. 8 for $E_\mathrm{s}/N_0 \mathrel{\widehat{=}} 34$ dB. In case of noncoherent detection, the same effects as in Fig. 6 are visible. When the middle user (■) moves closer to the other users, the performance worsens due to the overlap in the PSPs. A similar behavior to that of Fig. 7, where coherent detection without the EM lens performs better than that with the EM lens. When the EM lens is present, when the users are located in the same position, a performance loss is seen instead of having complete detection failure.

For noncoherent detection, the PSPs of the users overlap earlier than in the single-path scenario. This is a direct result of the broadening of the footprint caused by the spreading of the angle of arrival (cf. Sec. II-C).

C. Lens Focusing Parameter

For the chosen lens parameter $\Delta = 3\lambda$, the channel diversity is not fully exploited; it is possible to increase the gain by enlarging the footprint of the induced signal by increasing Δ.

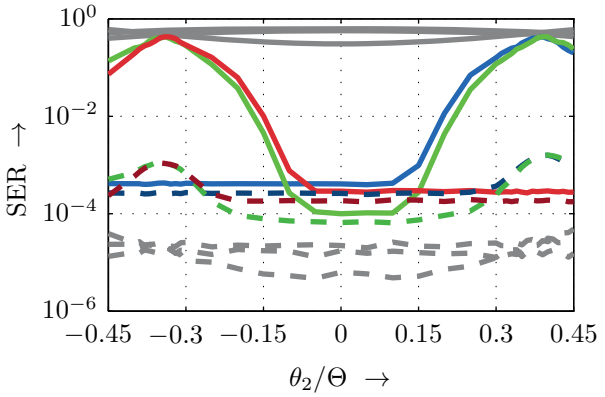

Figure 8. Symbol error rate vs. θ_2/Θ for the multi-user scenario. $N_\mathrm{u} = 3$. Two-path model. Inter-antenna spacing $d_\mathrm{a} = \lambda/2$. $\Delta = 3\lambda$. $E_\mathrm{s}/N_0 \mathrel{\widehat{=}} 34$ dB. user 1 (■): $m_1 = 20$ ($\theta_1 = -0.34\Theta$), user 3 (■): $m_3 = 85$ ($\theta_3 = 0.39\Theta$). The position of user 2 (■) is varied between -0.45Θ to 0.45Θ. Solid: DFDD (noncoherent); dashed: MRC (coherent). Gray plots are for the system without the EM lens.

To that end, simulations using the single-user two-path channel model and the multi-user two-path one were conducted. In the single-user case (■), the results are based on the middle user (i.e., user 2 (■)) where the aperture loss is zero.

The footprint is varied from $\Delta = 1\lambda$ to 15λ; the symbol error rate for $E_\mathrm{s}/N_0 \mathrel{\widehat{=}} 34$ dB is plotted in Fig. 9.

In the single-user case, as Δ increases, the symbol error rate for both noncoherent and coherent detection slightly decreases. This is expected, as now there is an increase in the number of observations of the signal. In the multi-user case, coherent detection performs similarly; the larger the footprint, the better the performance. However, for noncoherent detection, first a decrease in the error rate is seen, then beyond $\Delta = 5\lambda$, the performance starts to degrade. This comes from the overlap in the PSPs; spatial separation is lost and therefore, inter-user interference occurs.

ISBN 978-3-8007-4862-4

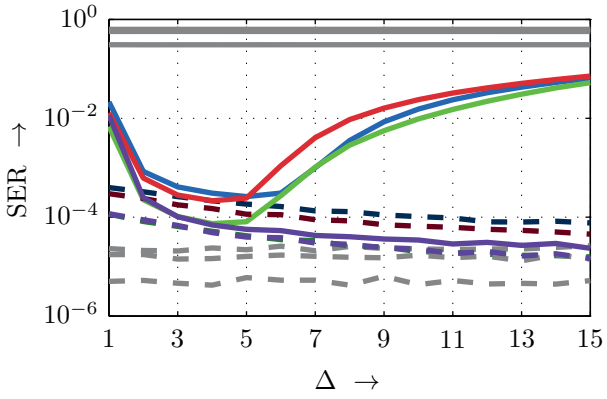

Figure 9. Symbol error rate vs. Δ. Two-path model. Inter-antenna spacing $d_{\mathsf{a}} = \lambda/2$. $E_{\mathsf{s}}/N_0 \mathrel{\widehat{=}} 34$ dB. The footprint is varied from $\Delta = 1\lambda$ to $\Delta = 15\lambda$. user 1 (■): $m_1 = 20$ ($\theta_1 = -0.34\Theta$), user 2 (■): $m_2 = 50$ ($\theta_2 = 0$), user 3 (■): $m_3 = 85$ ($\theta_3 = 0.39\Theta$). Solid: DFDD (noncoherent); dashed: MRC (coherent). Gray plots are for the system without the EM lens. Single-user case plotted in (■).

Hence, a trade-off between single- and multi-user performance exists: the wider the footprint, the better the per-user symbol error rate. However, when it comes to the multi-user case, unless the users are located far enough from each other, there will be an overlap in the PSPs and hence, a performance loss. This provides a design parameter to tune when deploying such a system.

In the scenario at hand (inter-antenna spacing, user location, SNR), choosing $\Delta = 5\lambda$ gives the optimum trade-off between per-user and multi-user performance.

V. Conclusion

In this paper, we have assessed an EM-lens-based antenna array system combined with noncoherent detection for the massive MIMO uplink scenario. We first stated a far-field-based model for the single-path and multi-path scenario. Simulation results highlighting the effectiveness of noncoherent detection when compared to coherent detection in the EM-lens-based system are presented. The plots also showed the effect of user positioning, which degrades when the user moves away from the array boresight. The performance decrease is due to the aperture loss of the array.

We also studied the effect of the EM-lens footprint on the simulation results. By increasing the footprint, the per-user performance is improved. However, the wider footprint may result in an overlap of the user-specific power-space profiles, which in turn increases the inter-user interference. In that case, a mechanic to resolve the interference, such as noncoherent decision-feedback equalization is required. This presents a design trade-off, where the system can be tuned towards per-user or multi-user performance. The choice depends on the position statistics of the users. When the users are always sufficiently spaced, an EM-lens with a larger footprint is more beneficial.

References

[1] F. Adachi, M. Sawahashi. Decision-Feedback Multiple-Symbol Differential Detection for Mary DPSK. *Electronics Letters*, vol. 29, no. 15, pp. 1385–1387, July 1993.

[2] M.A. Al-Joumayly, N. Behdad. Wideband Planar Microwave Lenses Using Sub-Wavelength Spatial Phase Shifters. *IEEE Transactions on Antennas and Propagation*, vol. 59, no. 12, pp. 4542–4552, Dec. 2011.

[3] B. Chantraine-Barès, R. Sauleau, L. Le Coq, K. Mahdjoubi. A New Accurate Design Method for Millimeter-Wave Homogeneous Dielectric Substrate Lens Antennas of Arbitrary Shape. *IEEE Transactions on Antennas and Propagation*, vol. 53, no. 3, pp. 1069–1082, Mar. 2005.

[4] O. Elijah, C.Y. Leow, T.A. Rahman, S. Nunoo, S.Z. Iliya. A Comprehensive Survey of Pilot Contamination in Massive MIMO–5G System. *IEEE Communications Surveys & Tutorials*, vol. 18, no. 2, pp. 905–923, 2016.

[5] R.F.H. Fischer, M. Bense. Noncoherent Decision-Feedback Equalization in Massive MIMO Systems. In *Proceedings of International Zurich Seminar (IZS)*, pp. 112–115, Zurich, Switzerland, Feb. 2014.

[6] T.L. Marzetta. Noncooperative Cellular Wireless with Unlimited Numbers of Base Station Antennas. *IEEE Transactions on Wireless Communications*, vol. 9, no. 11, pp. 3590–3600, Nov. 2010.

[7] B. Ottersten. Array Processing for Wireless Communications. In *Proceedings of 8th Workshop on Statistical Signal and Array Processing*, Corfu, Greece, June 1996.

[8] F. Rusek, D. Persson, B.K. Lau, E.G. Larsson, T.L. Marzetta, O. Edfors, F. Tufvesson. Scaling Up MIMO: Opportunities and Challenges with Very Large Arrays. *IEEE Signal Processing Magazine*, vol. 30, no. 1, pp. 40–60, Jan. 2013.

[9] R. Sauleau, B. Barès. A Complete Procedure for the Design and Optimization of Arbitrarily Shaped Integrated Lens Antennas. *IEEE Transactions on Antennas and Propagation*, vol. 54, no. 4, pp. 1122–1133, Apr. 2006.

[10] A. Schenk, R.F.H. Fischer. Noncoherent Detection in Massive MIMO Systems'. In *Proceedings of International ITG/IEEE Workshop on Smart Antennas*, Stuttgart, Germany, Mar. 2013.

[11] A.M. Tulino, A. Lozano, S. Verdú. Impact of Antenna Correlation on the Capacity of Multiantenna Channels. *IEEE Transactions on Information Theory*, vol. 51, no. 7, pp. 2491–2509, July 2005.

[12] G. Yammine, R.F.H. Fischer, C. Waldschmidt. On the Influence of the Antenna Pattern in Noncoherent Massive MIMO Systems. In *Proceedings of The Twelfth International Symposium on Wireless Communication Systems*, Brussels, Belgium, Aug. 2015.

[13] Y. Zeng, R. Zhang, Z.N. Chen. Electromagnetic Lens-Focusing Antenna Enabled Massive MIMO: Performance Improvement and Cost Reduction. *IEEE Journal on Selected Areas in Communications*, vol. 32, no. 6, pp. 1194–1206, Jun. 2014.

[14] Y. Zeng and R. Zhang. Cost-Effective Millimeter-Wave Communications with Lens Antenna Array. *IEEE Wireless Communications*, vol. 24, no. 4, pp. 81–87, Aug. 2017.

[15] P. Zetterberg. *Mobile Cellular Communications with Base Station Antenna Arrays: Spectrum Efficiency, Algorithms and Propagation Models.*, PhD Thesis. Royal Institute of Technology, Sweden, 1997.

ISBN 978-3-8007-4862-4